Sustainable synthesis of oxalic acid from C6 by using Fe@CNT based catalysts in mild conditions

Maria Ventura,[a] David Williamson,[b] Francesco Lobefaro,[c] Matthew Jones,[b] Davide Mattia,[b] Michele Aresta[a,b,] and Angela Dibenedetto,[a,d* c]

a. CIRCC, Via Celso Ulpiani, 27, 70126 Bari, Italy; b. Centre for Advanced Separations Engineering and Department of Chemical Engineering, University of Bath, Claverton Down, Bath BA2 7AY, United Kingdom; c. IC2R, Viale Enaudi 25, 70125 Bari, Italy; d. Department of Chemistry, University of Bari, Campus Universitario, 70126 Bari, Italy

Introduction:

The petrochemical industry has contributed to worldwide economic development over the past 150 years or so, but several serious environmental problems are associated with it. The need to establish environmentally friendly chemical processes is a must now and requires the development of novel and cost-effective methods to pollution prevention.[1] In recent decades, the substitution of non-renewable fossil resources such as crude oil, coal, and natural gas by renewable-carbon such as biomass, including lignocellulose and oil, (or even CO_2) as a sustainable feedstock has been extensively investigated for the manufacture of biofuels, commodity chemicals,[2] high added-value products and new bio-based materials such as bioplastics.[3] Among the renewable feedstock, lignocellulosic biomass has attracted considerable attention because its potential as a source of a wide range of platform chemicals like C6-polyols,[4] 5-hydroxymethylfurfural (5-HMF),[5] levulinic acid (LA)[6] or formic acid (FA).[7] Among these chemicals, 5-HMF, that is synthetized by dehydration of fructose, or even directly from glucose,[8] is considered one of the most important building-block intermediates. Its furan structure with an aldehydic and a hydroxyl moiety, has the potential to be transformed into numerous high value chemicals that can replace their analogues synthesized from fossil feedstock (Scheme 1).

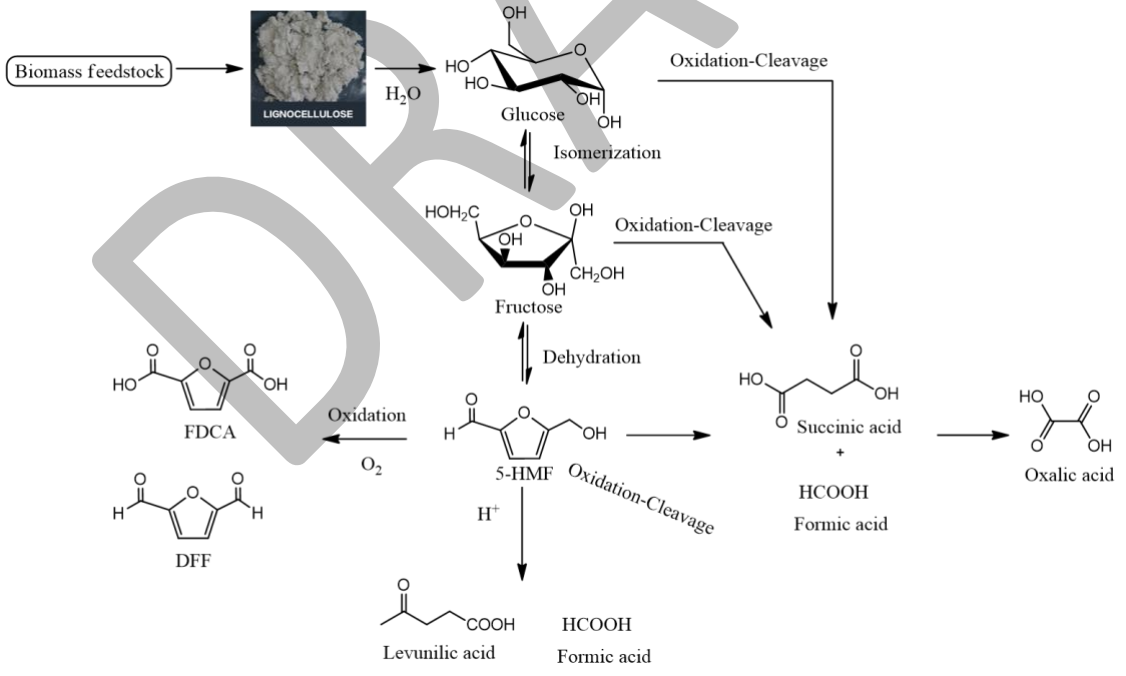

Scheme 1. Representative processes for biomass conversion into chemicals

Although the oxidation-cleavage of either 5-HMF or glucose, can be a sustainable method to produce important platform chemicals such as lactic acid (LA)[9] or oxalic acid (OA),[10] to date such route has not attracted much attention because the difficulty to selectively perform the process. Oxalic acid, and its derivatives have widespread industrial application in several fields such as textiles, tanning, oil refining, catalyst preparation, pharmaceuticals, dyes, explosives,

straw bleaching, printing, marble polishing, and metal and cloth cleaning.[10] It is also a very important chemical in petroleum, rare-earth, inks, rust and corrosion inhibitor, and dental adhesive processing.[11] Currently, the methods for producing OA are classified according to the starting raw material: ethene, ethene glycol, propene, lignin, molasses, sugarcane, sugars, flour, plant wastes, formate, carbonate and bicarbonate salts etc. Such methods are classified in six groups, i.e.: (i) fusion of sawdust with caustic soda, (ii) oxidation of olefins and glycols, (iii) radiation processing of carbonate solutions and molasses, (iv) fermentation of carbohydrates, (v) oxidation of carbohydrates by nitric acid, and (vi) decomposition of formates. The last three are widely used. Fermentative production of OA has been studied with renewed interest in the last decade, getting mainly citric acid and/or OA from sucrose and lactose depending on the fermentation conditions. High production of OA (>200 mM) has been reached, however a strict control on the pH is required to accumulate the acid, even in a low concentration,[12] making somehow complex such technology. The oxidation of carbohydrates by nitric acid is currently the industrial method to OA. A strong acid solution composed by HNO_3 and H_2SO_4 together with V_2O_5 as catalyst is used reaching a conversion of 99% with yields of OA from 2.9% to 54% and produces large volumes of waste.[13] Coupling of formats is an attractive route[11, 14] which, nevertheless, does not avoid the use of strong acid media. From an environmental point of view the above routes do not follow the 12 principles of green chemistry. We have recently developed selective, tunable and reusable heterogeneous catalysts for the aerobic oxidation of 5-HMF in water, avoiding the use of external additives and organic solvents that generate undesired waste.[15] Carbon nanotubes (CNTs) are a new kind of carbon materials that offer interesting possibilities as support for metal particles, due to the sp^2 carbon-constructed surface, the excellent electron transport performance and the electronic interaction of active nanoparticles with the CNTs walls.[16] In the field of biomass transformation, it has been proved that metal nanoparticles on CNTs are active in a wide range of conversions. In one of the most recent works, it has been reported that Au-Pd nanoparticles deposited on CNTs show higher catalytic activity than on other supports, like alumina or silica for the base-free aerobic oxidation of 5-HMF towards FDCA.[17] Therefore, CNTs can be considered a promising supporting material for catalysts to be employed in the oxidation of 5-HMF. Accordingly, we present in this paper the use of M@CNTs (M=Fe, V) or M@NCNTs (where NCNT is a nitrogen modified CNT) for the synthesis of oxalic acid from 5-HMF or glucose under aerobic oxidation in water. To the best of our knowledge this is the first report on a sustainable synthesis of OA from 5-HMF or glucose.

Results and discussion:

1. Synthesis of the catalysts

a. Preparation of Fe@CNTs and Fe@NCNT

Fe@CNTs and Fe@NCNTs were prepared via a floating catalyst CVD method in a sealed quartz tube (25 mm ID, 28 mm OD x 122 cm Length), which was placed into a tube furnace to control the reaction temperature. During the reaction, a precursor solution (45 mL) was loaded into a 50 mL syringe, which was then placed onto a syringe pump for automated injection once the reactor had reached the desired reaction temperature. To synthesize Fe@CNTs, the precursor solution consisted of 1.0 g ferrocene (FcH) dissolved in 50 mL toluene (20 mg/mL). To synthesise Fe@NCNTs, toluene was replaced with acetonitrile in the precursor solution to act as a nitrogen source.

During synthesis, the quartz tube was purged with 50 sccm Ar as the furnace tube furnace ramped up to the desired reaction temperature of 790 °C at a rate of 5 °C/min. When the reaction temperature was reached, the desired precursor solution was injected at a rate of 10 mL/hour for 4 hours under a flow of 50 sccm H_2 and 400 sccm Ar. The quartz tube was then left to cool to room temperature before the fresh catalyst was collected as a

black, powdery material via scratching the quartz tube interior with an elongated spatula. This typically provided a yield of ca. 1.4 g catalyst per synthesis.

b. Vanadium doping

To achieve 0.5 wt. % vanadium doping, 0.013 g $VO(acac)_2$ was dissolved in 15 mL methanol. 0.5 g fresh catalyst was then added to this solution to produce a dark slurry, which was stirred at room temperature for 24 hours. After stirring, the methanol had typically evaporated completely and the dry, doped catalyst could be easily collected.

c. Catalyst activation

Previous studies have shown that, immediately after synthesis, the iron nanoparticles embedded in the walls of the Fe@CNTs and Fe@NCNTs are obscured by a graphitic carbon layer. This prevents them from participating as catalytic sites. In order to expose these iron particles, the graphitic carbon layer must be removed via thermal oxidation in air, without damaging the CNT support structure. This was achieved by packing 0.45 g catalyst into a ¼" x 12.5 cm stainless steel tube, which was loosely packed with quartz wool at the bottom to allow for air flow while preventing the catalyst from escaping. For Fe@CNT based catalysts, the catalyst was heated in a muffle oven at 570 °C for 40 minutes, ramping up at a rate of 10 °C/min. For Fe@NCNTs, the catalyst was activated at 400 °C for 1 hour, due to the decreased stability of the NCNT support structure after nitrogen doping. This thermal activation step was always carried out following the vanadium doping step.

2. Characterization of the catalysts.

A study on the BET surface area and acid-base properties of the different Fe@CNT(NCNT) used in the production of OA was carried out. Table 1 shows the BET surface area and the total and strong basic and acid sites (calculated from total area under the peaks in the TPD experiments), expressed through the volume of CO_2 and NH_3 uptake and release, respectively. The ratio of strong acid/basic sites has been also calculated (n_a/n_b).

Table 1. BET surface area and basicity/acidity strength of different Fe@CNT.

Entry	Solid	Total V CO_2 adsorbed (mL/g)	Strong CO_2 adsorption (mL/g)	Total V NH_3 adsorbed (mL/g)	Strong NH_3 adsorption (mL/g)	n_a/n_b	BET surface area (m^2/g)
1	Fe@CNT	0.551	0.550	2.254	1.987	3.6	78.33
2	Fe@NCNT	0.397	0.385	1.938	1.847	4.6	81.46
3	FeV@CNT	1.593	1.459	3.849	3.613	2.5	81.37

A comparison between Entries 1 and 2 reveals that when nitrogen is inserted into the CNTs, a drop in both acid and basic sites was observed resulting in an increase in the ratio n_a/n_b. Different behaviour was observed when vanadium was included in the catalysts: huge increase in both acid and basic sites was observed with a resulting lower ratio n_a/n_b. Concerning the BET surface area, no major differences were observed for the three solids, Fe@CNT, Fe@NCNT, FeV@CNT.

The redox behaviour was investigated by H_2-TPR analysis. Figure 1a displays the H_2 consumption profile for Fe_2O_3, 1b V_2O_5, 1c Fe@CNT, 1d Fe@NCNT and 1e for FeV@CNT.

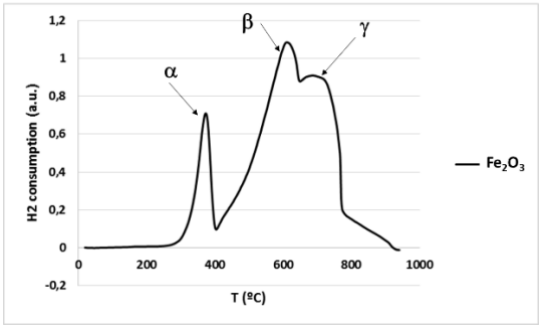

Figure 1a. H_2-TPR profile for Fe_2O_3

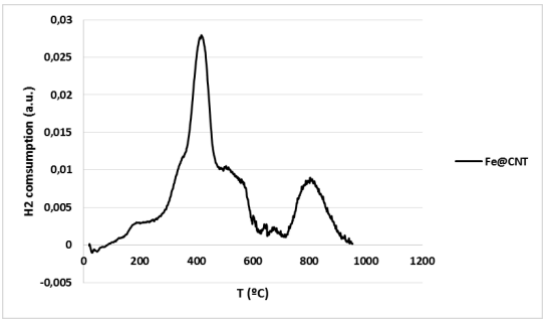

Figure 1b. H_2-TPR profile for Fe@CNT

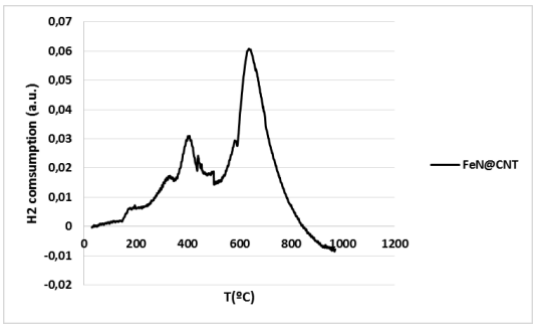

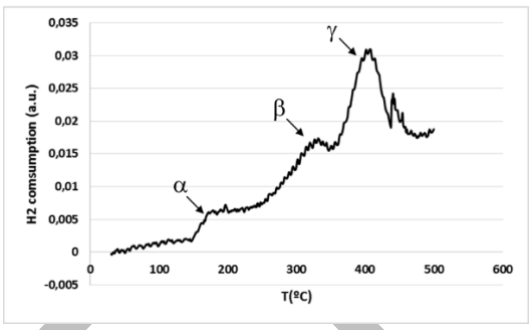

Figure 1c. H_2-TPR profile for Fe@NCNT and its magnified region from 0 to 500 ºC

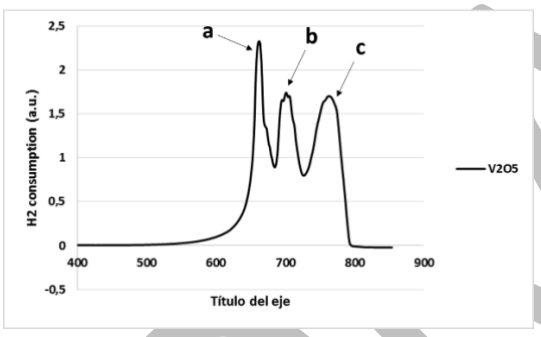

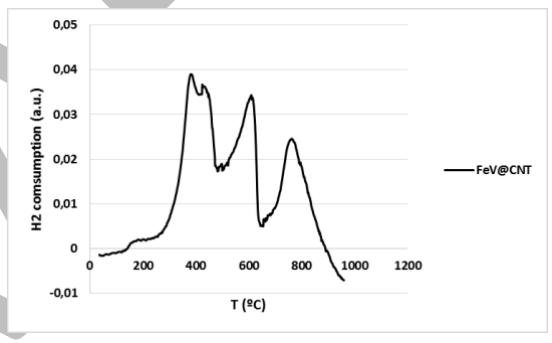

Figure 1d. H_2-TPR profile for V_2O_5 **Figure 1e.** H_2-TPR profile for Fe,V@CNT

Generally, the reduction of pure Fe_2O_3 to metallic iron can be expressed by the following consecutive transitions: $Fe_2O_3 \rightarrow Fe_3O_4 \rightarrow FeO \rightarrow Fe$[18] that are identified in the profile shown in Fig.1a, as α = 370 °C, β = 619 °C , γ = 707.1 °C.[18-19] As displayed in Fig.1b, H_2-TPR profiles for the sample Fe@CNT show two reductive peaks centred at about 420 ºC and 800 ºC, respectively. The low temperature peak is likely due to the reduction of Fe^{3+} species to metallic Fe. The high temperature peak can be assigned to the reduction of carbon species on the surfaces of CNTs.[16, 20] It can be noted that in Fe@CNT sample the three peaks assigned to the three transitions of Fe species, collapse in only one reduction peak. It is possible to identify another reduction peak at low temperature ~185 ºC. These facts imply that the confinement of Fe inside the CNTs pore results in a easier reduction. The sample Fe@NCNT shows three peaks in the magnified region at 186, 338 and 400 ºC, located at lower temperature than in pure Fe_2O_3. This is an evidence of the different interaction of Fe with NCNTs than with CNTs.

H_2-TPR profile for pure V_2O_5, Fig. 1d, shows three reduction peaks, a = 662 ºC, b = 403 ºC, c = 764 ºC associated to the transitions: $V_2O_5 \rightarrow V_6O_{13} \rightarrow V_2O_4 \rightarrow V_2O_3$ [21]. In an attempt to attribute the relevant transitions to Fe or V (Fig.1e), the peak at lowest reduction temperature centred at 386 ºC is tentatively attributed to the transitions belonging to Fe and the other two to the transitions of V. Both values are present at lower temperatures than in pure oxides.

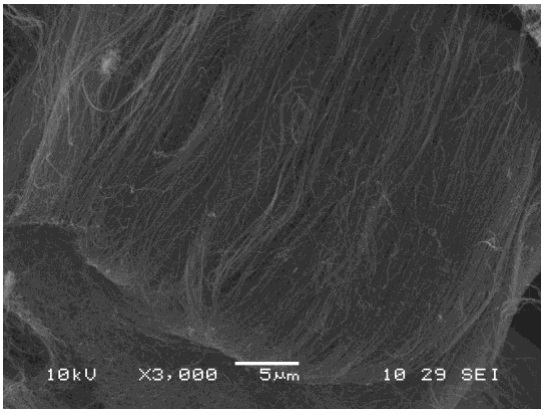

Figure x: SEM micrographs of Fe@CNTs confirming the presence of aligned bundles of tubular structures.

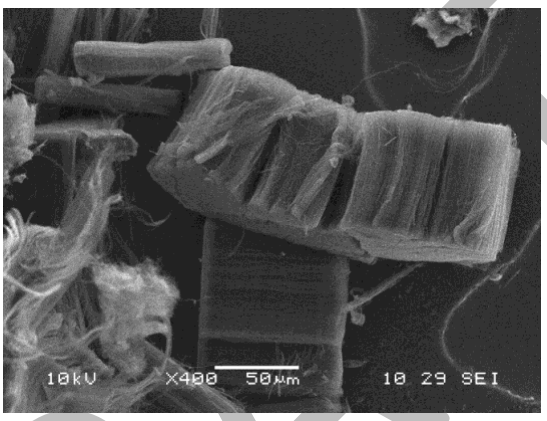

Figure x

doping, with iron particles clearly adorning the tube walls, similar to the Fe@CNTs.

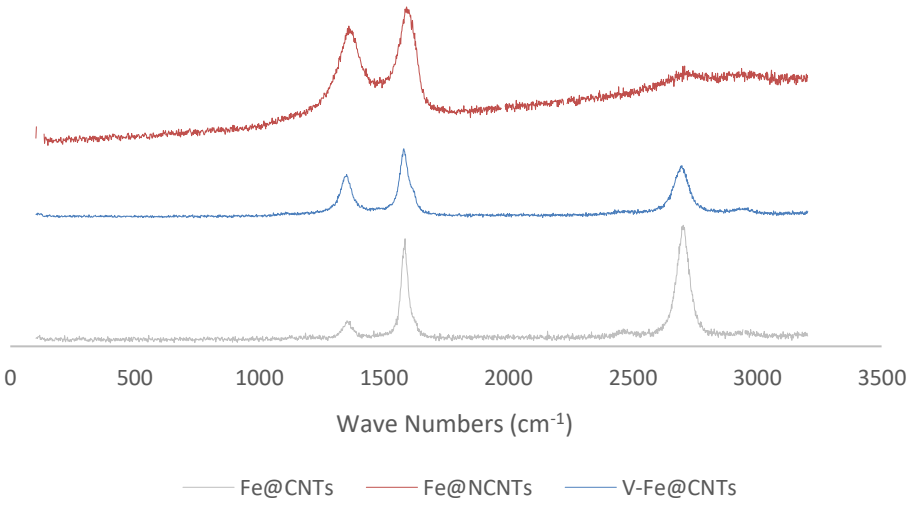

Figure x: Raman spectra of activated Fe@CNTs, Fe@NCNTs, and V-Fe@CNTs. All spectra are acquired following the activation step to remove the graphitic carbon layer obscuring the iron particles.

The small D and large G and G' peaks observed in Fe@CNTs indicate good purity and long-range order in the CNT support structure. Conversely, the increased I_D/I_G ratio and suppressed G' peak observed in Fe@NCNTs is clearly indicative of defects and loss of long-range order as a result of nitrogen doping. V-Fe@CNTs appear to experience some increased disorder as a result of the vanadium doping process, though a degree of long-range order is maintained. This is confirmed by the presence of the G' peak at ca. 2788 cm^{-1}. The I_D/I_G ratios of each sample have been calculated for comparison in Table x.

Table x: The calculated I_D/I_G ratios of Fe@CNTs, Fe@NCNTs, and V-Fe@CNTs following activation to remove the graphitic carbon layer.

Sample	I_D/I_G
Fe@CNTs	0.19
V-Fe@CNTs	0.69
Fe@NCNTs	0.91

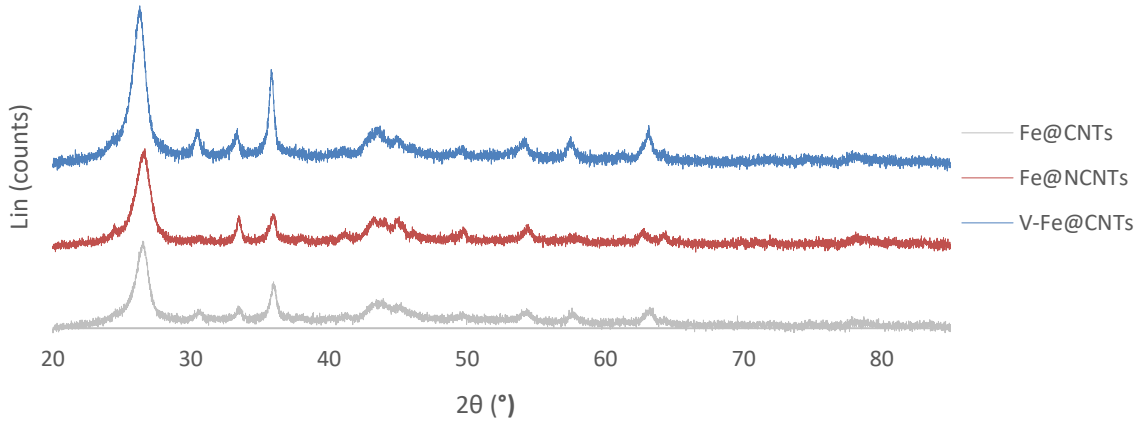

Figure x: The XRD spectra of Fe@CNTs, Fe@NCNTs, and V-Fe@CNTs following activation.

XRD analysis of Fe@CNTs, Fe@NCNTs, and V-Fe@CNTs was conducted prior to reaction. All materials displayed a strong peak at 26.2°, which is indicative of the CNT support structure. Peaks at 30.4 °, 35.8 °, 43.2°, 54.3 °, 57.8 °, and 62.8 ° all indicate the expected presence of Fe_2O_3 in all samples, though they are less pronounced in the Fe@NCNTs. This is likely due to the lower activation temperature employed to remove the graphitic layer from the catalytic nanoparticles (400 °C compared to 570 °C), resulting in less complete oxidation of the iron. Peaks at 35.8 °, 43.2 °, 57.8°, and 64.2 ° all indicate the presence of Fe_3O_4 in all samples. Overlapping peaks at 43.2 °, 44.0 °, and 45.0 ° with a small shoulder peak at 41.2 ° indicate the presence of iron carbides such as Fe_3C and Fe_5C_2, with Fe_3C being the most likely to occur. These peaks appear more defined in the Fe@NCNTs once again due to the lower activation temperature used, resulting in less oxidation of the iron, which has been shown elsewhere to exist mostly as metallic iron, iron carbides and iron nitrides prior to activation in air. The harsher activation conditions used on Fe@CNT and V-Fe@CNTs thus convert more of the initial carbide phase into the oxide.

These overlapping peaks may contain traces of peaks for the iron nitride $Fe_{15}N_2$ in the Fe@NCNTs (expected at 42.5 ° and 45.0 °), though they are difficult to distinguish, and the lack of additional, smaller nitride peaks at 59.0 °, 65.5 °, 77.5 ° and 81.0 ° indicates that the nitride has been largely removed by the activation process. Carbide is more likely to remain

due to the much higher relative concentration of carbon to nitrogen in the CNT support structure (ca. 95 at. % C versus 3 at. % N as has been confirmed via XPS in other work).

3. Results and discussion

a. Reaction of oxidation of 5-HMF.

The formation of oxalic acid by oxidation-cleavage of 5-HMF was investigated using the three catalysts, Fe@CNT, Fe@NCNT and Fe,V@CNT in water using O_2 as oxidant, minimizing in this way the waste generated in the process. First, the catalytic activity was evaluated using Fe@CNT: the results are reported in Table 1.

Table 1. Oxidative cleavage of 5-HMF using Fe@CNT as catalyst.

					Selectivity (%)							
Entry	rpm	Time (h)	T (K)	Conv.(%)	DFF	FFCA	FDCA	FA	LA	OA	SA	Fructose
1	1000	6	383	23.7	4.41	89.6	0	5.1	5.6	0	0	0
2	1000	6	403	99	0.39	18.8	22.2	8.5	0	22.03	8.58	38.94
3	500	6	403	99	4.6	2.35	0	23.3	0	30.6	23.3	23.3
4	250	6	403	99	3.2	4.8	0	18.5	0	35.8	6.6	17.7
5	250	6	413	99	0	4.1	0	29.4	0	28.4	7.8	9.2

Reaction conditions:$[5\text{-HMF}]_i$=0.16M; 0.025g of catalyst; P_{O_2} = 1 MPa; rpm: stirring speed per min.

The effect of temperature, under 1000 rpm stirring, was first evaluated as shown in Table 1, Entries 1, 2. The conversion of 5-HMF increases from 23.7 % to 99 % with rising from 383 K to 403 K the temperature, while the selectivity towards OA increases from 0% to 22.03%. Thus, 403 K was selected as the operative temperature. Other products (i.e., SA) were also detected in the reaction mixture as a result of un-complete cleavage.

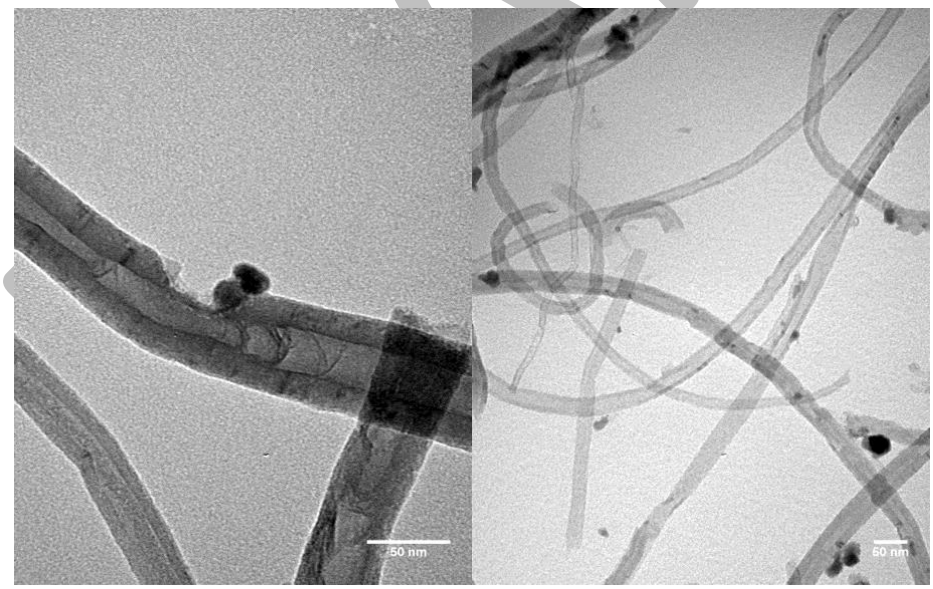

Figure x: TEM micrographs of MA110 and MA130 indicating tube degradation after reaction. Nanoparticles are observed to be torn out of the tube wall, and the tube walls themselves snapped or deteriorated.

At 1000 rpm, leaching of Fe from CNTs was observed and the breaking of CNTs detected by TEM experiments. We decided, thus, to decrease the stirring speed and modify the geometry of the stirring bar (from a linear bar to a round bottom magnet with a toping star for better mixing at lower speed) in order to improve the stability of the catalyst. When the rpm was decreased from 1000 to 500 the selectivity towards OA increased to 30.6 %, Entry 3.

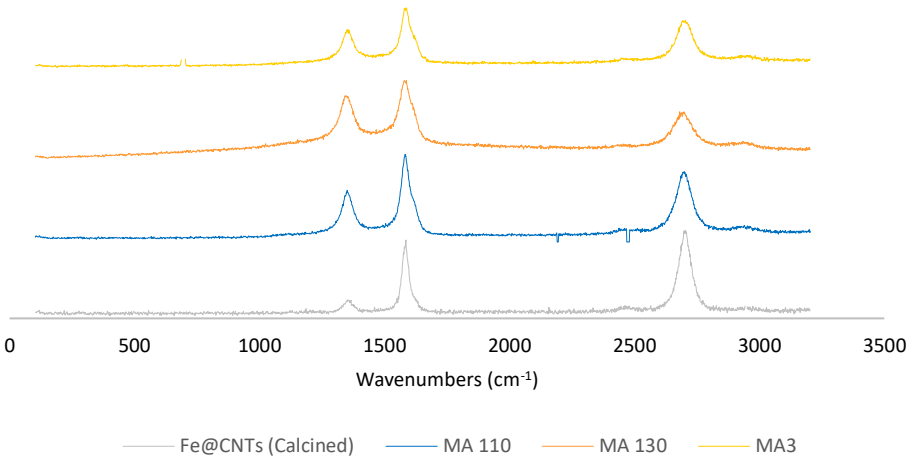

Figure x: Raman spectra of Fe@CNT catalysts pre- and post-reaction at under varying conditions. The increase in the I_D/I_G ratio observed indicates some damage occurs to the CNT structure during reaction. Increasing the temperature to 130 °C from 110 °C results appears to result in more damage to the CNT structure, however lowering the rate of stirring in MA3 serves to reduce the damage caused. This can be corroborated from the calculated I_D/I_G values displayed in Table x.

Table x: The calculated ratios of the D and G peaks of Raman spectra detailed in Figure x. An increase in I_D/I_G indicates increased disorder in the sample, caused by defects or damage in the CNT support structure.

Sample	I_D/I_G
Fe@CNT Calcined	0.19
MA110	0.59
MA130	0.82
MA3	0.65

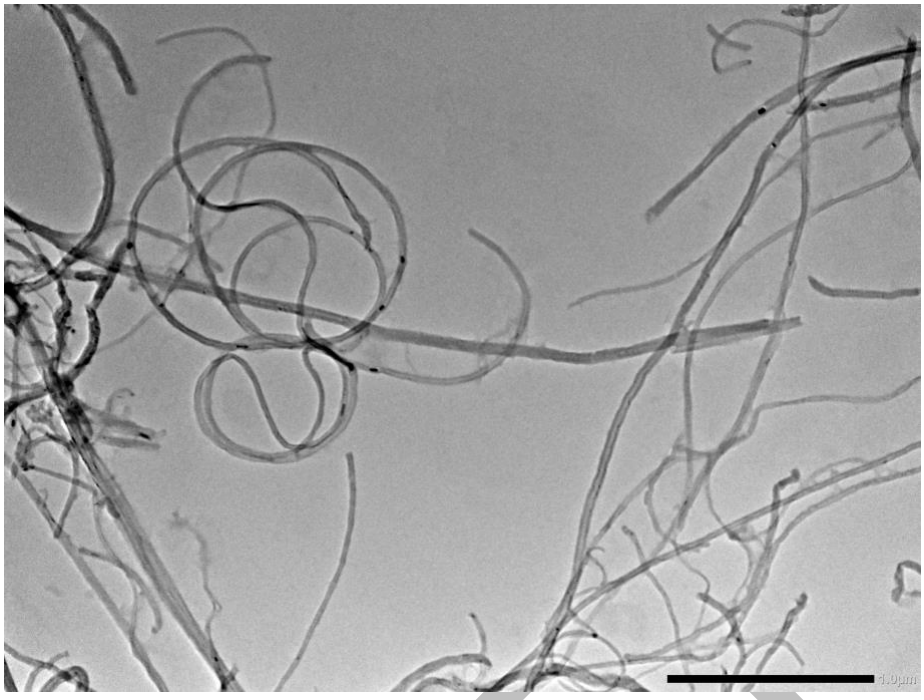

Figure x: TEM of MA3, displaying some damage to the CNT structure, though less than is observed in MA1 and MA2, which is supported via Raman analysis.

Decreasing even more the rpm, the selectivity towards OA increased to 35.8% while the stability of the catalyst neatly increased as shown by TEM. In order to investigate the role of the temperature when 500 rpm was fixed as the optimal velocity, an experiment was performed at 413 K, Entry 5, Table 1. The selectivity towards OA decreased from 35.8% to 28.4 % while the selectivity towards FA increased from 18.5% to 29.4%. It is clear that increasing the temperature causes the cleavage of the C-C bond converting OA into FA.

The effect of the oxygen pressure was also investigated, and the results are shown in Table 2.

Table 2. Oxidative-cleavage of 5-HMF at different oxygen pressures.

					Selectivity(%)						
Entry	Rpm	Time (h)	PO_2 bar	Conv.(%)	DFF	FFCA	FA	LA	**OA**	SA	Fructose
1	250	6	5	65.2	0	0	41.7	5.3	**25.1**	14.1	11.7
2	250	1.5	10	91	8.04	4.1	19.8	4.1	**38.4**	7.1	12.5
3	250	1.5	20	99	1.6	0	40.6	0	**35.9**	9.9	11.8

Reaction conditions:$[5\text{-HMF}]_i$=0.16M, 0.025g of catalyst, T = 403K

Noteworthy, either increasing the pressure from 10 to 20 bar or decreasing it to 5 bar has a negative effect on the selectivity of OA since it is anyway decreased. The lowest pressure caused an uncomplete cleavage, and the selectivity towards SA was the highest, Entry 1. On the other hand, when 20 bar were used the selectivity towards SA decreased in favour of FA, Entry 3. The optimal pressure is thus 10 bar that minimizes the formation of both SA and FA, Entry 2. We have carried out a kinetic study in order to know if OA is degraded to FA as the reaction time increases. The study was performed at two temperatures: 403 K (Figure 2a), and 413K (Figure 2b). The selectivity towards OA was decreased after 3h at 403K or after 1.5h at 413K. At the same time the selectivity towards FA increased with the temperature, showing that OA is degraded to FA in time.

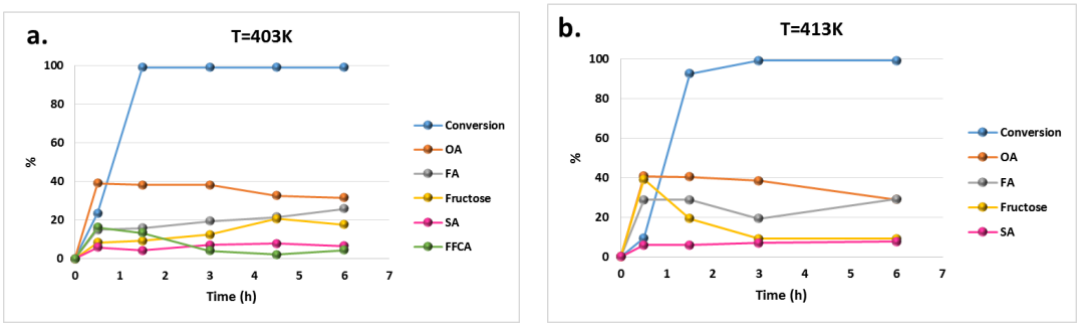

Figure 2. Kinetic study on the oxidation-cleavage of 5-HMF at: a. 403K; b. 413K

It is worth noting that the conversion of 5-HMF was almost quantitative in both reactions. However, the selectivity towards oxalic acid reaches its maximum value after 1.5 h of reaction at 403 K and after 30 min at 413 K. For longer times, OA is degraded to FA, whose selectivity increases from 19.4 to 25-28%. Obviously, the conversion of 5-HMF decreases at shorter times: from 99 after 3 h to 9.5 % after 30 min. In conclusion, the best conditions for maximizing the conversion of 5-HMF and the formation of OA are 1.5 h at 403 K.

We have compared the activity of Fe@CNT to those of Fe@NCNT and Fe,V@CNT, Table 3. Comparing Fe@CNT (Entry 2, Table 2) with Fe@NCNT (Entry 2, Table 3), one can see that there are no major changes in the selectivity towards OA in the same reaction conditions, but the global conversion of 5-HMF is lower when Fe@CNT is used. This can be a consequence of the increased value of n_a/n_b from 3.6 for Fe@CNT to 4.6 for Fe@NCNT. Noteworthy, a significant rehydration to fructose is observed with Fe@NCNT.

However when Fe,V@CNT was used significant changes on the product distribution was observed: after 6h FFCA was the major product of the reaction, Entry 4. When the reaction was performed for longer reaction time, 12h Entry 5, FA was obtained as the major product (84.3%) of the reaction making such reaction an interesting route to FA from C6 polyol. The presence of Vanadium makes lower the reduction temperature, Fig.1e: therefore, the oxidative cleavage is easier and FA is obtained that is the pre-ultimate product in the oxidative-cleavage chain that terminates with CO_2 formation.

Table 3. Oxidative-cleavage of 5-HMF using Fe@NCNT or Fe,V@CNT.

				Selectivity (%)						
Entry	Catalyst	Time (h)	Conv.(%)	DFF	FFCA	FA	LA	**OA**	SA	Fructose
1	Fe@NCNT	3	47.8	11.7	0	26.5	0	**39.8**	0	21.8
2		6	90.2	4.9	0	37.03	0	**37.9**	6.2	4.1
3	FeV@CNT	1.5	62.1	3.3	61.8	10.8	2.7	**19.9**	1.4	0
4		6	99	0	65.1	25.1	0	**6.3**	3.5	0
5		12	99	0	0	**84.3**	8.3	**0**	5.07	0

Reaction conditions:$[5\text{-HMF}]_i$=0.16M, 0.025g of catalyst, T = 413K.

b. Reactions using Glucose as substrate.

The catalysts were also tested using glucose Table 4, or fructose Table 5, as substrates. When Fe@CNT was used, Entry 1, no activity was observed even at a long reaction time or high temperature. However, when Fe@NCNT was used as catalyst, Entry 2, Glucose was converted to a mixture composed by OA, FA and SA with 4.2, 59.4, 23.6% of selectivity respectively. At longer reaction time, Entry 3, the conversion was increased from 17.3 to 22 %, at the same time the amount of FA was increased while the selectivity to OA was kept constant. SA was detected as intermediate of the reaction. At higher temperature, Entry 4, the conversion increased compared with the results shown in Entry 2 and the selectivity increased too.

Using Fe,V@CNT the conversion and yield of OA increase with the temperature, Entries 5-6, but huge amounts of FA and other compounds are formed.

Table 4. Reactions using glucose as substrate.

							Selectivity (%)				
Entry	Catalyst	Time (h)	T (K)	PO_2 bar	[Glucose]	Conv.(%)	FFCA	FA	**OA**	SA	Fructose
1	Fe@CNT	24	423	20	0.2	0	-	-	**-**	-	-
2	Fe@NCNT	6	403	20	0.2	17.3	32.9	29.4	**24.2**	23.6	0
3	Fe@NCNT	12	403	20	0.2	22.0	0	41.7	**27.01**	18.3	0
4	Fe@NCNT	6	423	20	0.2	21.8	0	16.4	**37.05**	17.3	29.3
5	VFe@CNT	12	403	20	0.2	36.8	12.9	50.1	**16.6**	7.7	12.2
6	VFe@CNT	12	423	20	0.2	79.6	29.7	41.8	**27.89**	15.4	0

The above data show that glucose can be used for the production of OA, but even if the selectivity is comparable to that found when 5-HMF is used (Entry 4), the conversion is much lower. Fructose is the product of isomerization of glucose and its presence in the reaction medium is a bit random.

c. The role of SA.

The analysis of the above data suggest that there is a stepwise cleavage of the starting C6-skeleton to a C4 (SA), C2 (OA) and C1 (FA). In order to understand whether SA is really an intermediate or is just a by-product, we have reacted SA with O_2 in presence and absence of FA and checked the formation of OA. Table 5 shows the results when fructose or SA were used as substrate. The reactions were performed using Fe@CNT as catalyst.

In the reaction performed with fructose at lower reaction time (1 h), low conversion was reached and a mixture of SA+FA was obtained. (Entry 1) After 6h, SA reacted and was transformed into OA, that suggests that OA is generated by oxidative-cleavage of SA. At longer reaction time, (Entry 3) fructose was completely converted to OA+FA, being the latter the major product in the reaction because is generated also from the degradation of OA.

Using SA as starting material, OA is generated within 1 h at 98% of selectivity at a low SA conversion, Entry 4. The conversion of SA does not increase even if the reaction is kept for a longer time (Entries 4-6). Conversely, if FA is added to SA, Entry 7, SA is selectively converted into OA. At longer reaction time, more than 12h, OA was degraded affording FA. This suggests that FA helps the cleavage of SA into OA.

Table 5. Reactions using fructose or SA as substrate.

							Selectivity (%)		
Entry	Catalyst	Time (h)	T (K)	Substrate	PO_2 bar	Conv.(%)	FA	OA	SA
1	Fe@CNT	1	403	Fructose	10	1.2	21.8	-	79.3
2	Fe@CNT	6	403	Fructose	10	30.5	27.3	46.5	26.3
3	Fe@CNT	36	403	Fructose	10	99	78.6	22.1	0
4	Fe@CNT	1	403	SA	10	1.2	0	98	0
5	Fe@CNT	6	403	SA	10	2.4	0	98	0
6	Fe@CNT	12	403	SA	10	2.5	0	98	0
7	Fe@CNT	12	403	SA+FA	10	12.5	0	99	0

Notes:

I think we can stop here with the paper, but several issues must be clarified, for which we need more catalysts Fe@CNT

Point for further research

Based on the above results, depicting a reaction pathway is only tentative as several issues need to be clarified such as:
1. Is glucose directly converted or 5-HMF is the starting molecule? 5-HMF is not observed when starting from Glucose
2. FFCA is an intermediate or a by-product?
3. FA helps the cleavage of SA: does it play any other role during the reaction.

FFCA was used as starting material, but the results are a bit strange.

Scheme 1. Plausible pathways for the oxidation-cleavage from 5-HMF.

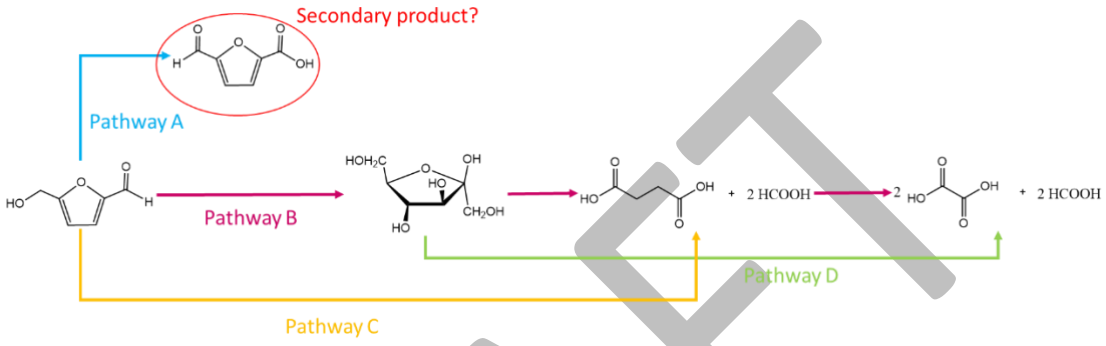

Bibliography:

[1] R. D. P. e. al, *Biomass as Feedstock for a Bioenergy and Bioproducts Industry: The technical Feasibility od a Billion-Ton Annual Supply*, **2005**.
[2] M. Ventura, A. Dibenedetto, M. Aresta, *Inorg. Chim. Acta* **2017**, *review, accepted*.
[3] Z. Zhang, K. Deng, *ACS Catalysis* **2015**, *5*, 6529-6544.
[4] Q. Xiang, Y. Y. Lee, R. W. Torget, in *Proceedings of the Twenty-Fifth Symposium on Biotechnology for Fuels and Chemicals Held May 4–7, 2003, in Breckenridge, CO* (Eds.: M. Finkelstein, J. D. McMillan, B. H. Davison, B. Evans), Humana Press, Totowa, NJ, **2004**, pp. 1127-1138.
[5] A. Dibenedetto, M. Aresta, L. d. Bitonto, C. Pastore, *Chem.Sus.Chem* **2016**, *9*, 118-125.
[6] F. D. Pileidis, M.-M. Titirici, *ChemSusChem* **2016**, *9*, 562-582.
[7] J. Yun, G. D. Yao, F. M. Jin, H. Zhong, A. Kishita, K. Tohji, H. Enomoto, L. Wang, *Aiche Journal* **2016**, *62*, 3657-3663.
[8] aA. A. Rosatella, S. P. Simeonov, R. F. M. Frade, C. A. M. Afonso, *Green Chem.* **2011**, *13*, 754-793; bX. L. Tong, Y. Ma, Y. D. Li, *Appl. Catal. A-Gen.* **2010**, *385*, 1-13; cA. Dibenedetto, M. Aresta, C. Pastore, L. di Bitonto, A. Angelini, E. Quaranta, *RSC Adv.* **2015**, *5*, 26941-26948.
[9] L. Li, F. Shen, R. L. Smith, X. Qi, *Green Chemistry* **2016**.
[10] *Economics of Oxalic acid from sugar, Vol. E251110A0*, **2017**.

[11] P. JC., *Oxalic acid, Vol. 9*, **1991**.
[12] aS. K. Mandal, P. C. Banerjee, *Process Biochem.* **2005**, *40*, 1605–1610; bS. H, B. W, S. F, *FEMS Microbiol Lett* **1994**, *119*, 365–370; cR. G. v. d. V. P. V. J., *Microbiology* **1999**, 2569–2576.
[13] aW. Guo, Jiang, H., Hague, Yuan. , *Manufacture of oxalic acid from beet waste slag by hydro-carbonylation at atmospheric pressure*, **1997**; bL. S. Richmond*, Vol. US3720591 A*, USA, **1973**; cE. Yonemitsu, T. Isshiki, T. Suzuki, Y. Yashima, in *U.S. Patent, Vol. 3,678,107* (Ed.: U. S. Patent), U.S, **1969**; dC. L. Mehltretter, C. E. Rist, *Journal of Agricultural and Food Chemistry* **1953**, *1*, 779-783.
[14] Radulescu G., M. M.-I., L. Cornos, G. Vapler*, Vol. RO106878 B1 30: 4* (Ed.: Rom.), **1993**.
[15] aM. Ventura, F. Lobefaro, M. Aresta, A. Dibenedetto, *Submitted* **2017**; bM. Aresta, A. Dibenedetto, M.Ventura*, Vol. patent filed*, Italy, **2017**; cM. Ventura, M. Aresta, A. Dibenedetto, *Chem.Sus.Chem* **2016**, *9*, 1096 – 1100.
[16] X. Guo, J. Guan, B. Li, X. Wang, X. Mu, H. Liu, *Scientific Reports Nature* **2015**, *5*, 16451.
[17] C. Zhou, W. Deng, X. Wan, Q. Zhang, Y. Yang, Y. Wang, *ChemCatChem* **2015**, *7*, 2853-2863.
[18] J. Zielinski, I. Zglinicka, L. Znak, Z. Kaszkur, *Appl. Catal. A: Gen.* **2010**, *381*, 191-196.
[19] W. K. Jozwiak, E. Kaczmarek, T. P. Maniecki, W. Ignaczak, W. Maniukiewicz, *Appl. Catal. A: Gen.* **2007**, *326*, 17-27.
[20] H. e. a. Yang, *J. Mol. Catal. A Chem* **2010**, *323*, 33-39.
[21] M. M. Koranne, J. G. Goodwin, G. Marcelin, *J. Catal.* **1994**, *148*, 369.